Wear-caused deflection evolution of a slide rail, considering linear and non-linear wear models

2017 J. Phys.: Conf. Ser. 843 012068

(http://iopscience.iop.org/1742-6596/843/1/012068)

IOP Conf. Series: Journal of Physics: Conf. Series **843** (2017) 012068 doi:10.1088/1742-6596/843/1/012068

Wear-caused deflection evolution of a slide rail, considering linear and non-linear wear models

Dongwook Kim[1], Luca Quagliato[2], Donghwi Park[1], Mohanraj Murugesan[1], Naksoo Kim[1] and Seokmoo Hong[3]

[1]Department of Mechanical Engineering, Sogang University, Seoul, 04107, Republic of Korea
[2]Department of Management and Engineering, University of Padua, Vicenza, I-36100, Italy
[3]Department of Metal Mold Design Engineering, Kongju National University, Cheonan, 32588, Republic of Korea

E-mail: nskim@sogang.ac.kr

Abstract. The research presented in this paper details an experimental-numerical approach for the quantitative correlation between wear and end-point deflection in a slide rail. Focusing the attention on slide rail utilized in white-goods applications, the aim is to evaluate the number of cycles the slide rail can operate, under different load conditions, before it should be replaced due to unacceptable end-point deflection. In this paper, two formulations are utilized to describe the wear: Archard model for the linear wear and Lemaitre damage model for the non-linear wear. The linear wear gradually reduces the surface of the slide rail whereas the non-linear one accounts for the surface element deletion (i.e. due to pitting). To determine the constants to use in the wear models, simple tension test and sliding wear test, by utilizing a designed and developed experiment machine, have been carried out. A full slide rail model simulation has been implemented in ABAQUS including both linear and non-linear wear models and the results have been compared with those of the real rails under different load condition, provided by the rail manufacturer. The comparison between numerically estimated and real rail results proved the reliability of the developed numerical model, limiting the error in a ±10% range. The proposed approach allows predicting the displacement vs cycle curves, parametrized for different loads and, based on a chosen failure criterion, to predict the lifetime of the rail.

1. Introduction

A slide rail is a linear guide composed of two or more members and several balls. When the slide rail is put in motion its members move forwards and backwards, and their sliding contact with the balls cause a progressive wear of the inner surface of the rails. The amount of wear progressively increases during the operational life time of the rail and, for different average applied loads, the rail experiences a failure for considerably different numbers of forward-and-backward cycles. The failure of the slide rail is normally identified by the condition for which, due to the progressive wear, the clearance between balls and rails increase to such a point that the end-point deflection of the last member of the rail makes the product, where the rail is installed, to be unusable.

In the literature, several contribution dealt with the sliding contact between objects, as follows. Singh et al. [1] studied the importance of coating and lubrication in the sliding contact, highlighting

how they can influence the lifetime of the considered product. Seo et al. [2] analyzed the different contribution of wear and fatigue in the resulting lifetime of two different railway steels, showing how different material are subjected, in a different way, to these two wearing effects. Yang et al. [3] utilized the Weibull distribution to predict the lifetime of slewing bearing by means of accelerated life testing. Maru et al. [4] studied the influence of possible contaminations in the lubricant those can make the bearing to fail earlier than its expected lifetime. In addition to that, several authors studied the influence of both vibrations and noise on the lifetime of the bearing, as here summarized. Nguyen et al. [5] used an empirical mode decomposition model for the detection of the vibration in the bearing systems which can indicated an incoming failure. Karacay et al. [6] studied the different signals produced by different defects those may occur in the bearing, developing a method which could also predict their position. Finally, by utilizing a non-linear dynamic numerical model, Singh et al. [7] analyzed the effect of the impulsive force has on the bearings and on the signals originated from their application. Concerning the lifetime prediction based on wear, Lee et al. [8] and Hwang et al. [9] utilized the accelerated life testing to predict the lifetime of roll bearing systems.

The present research work deals with the development a numerical model able to predict the cycle-based evolution of the end-point displacement of the last member of a slide rail, for different average operating loads, taking into account both linear and non-liner wear contributions, by utilizing two different wear models. Afterwards, based on a user-defined failure criterion, the number of cycles the slide rail can operate before it should be substituted can also be determined.

In order to determine the model constants to be utilized in both linear and non-linear wear model, a test machine replicating the operating conditions of the slide rail has been designed and build and simple tension test have been also conducted. Moreover, in order to validate the proposed numerical approach, the results of the numerical model have been compared with those of experiments conducted on real slide rails by the rail producer, showing the reliability of the developed approach in predicting the end-point displacement vs number of cycles, for different average loads. The developed approach is of very interest for the industrial compartment since it can be used to efficiently operate a predictive substitution of the slide rail after a certain amount of cycles, reducing the risk of critical failures of the products where they are installed.

2. The slide rail application

This study focuses on the development of a numerical model for the prediction of the end point deflection of a slide rail utilized in many white-goods application. In Figure 1 the real product, target of the study, is shown in both closed and opened configurations. In Figure 2, a schematic representation of the slide rail in opened and closed configuration and the detail of its cross-section are presented.

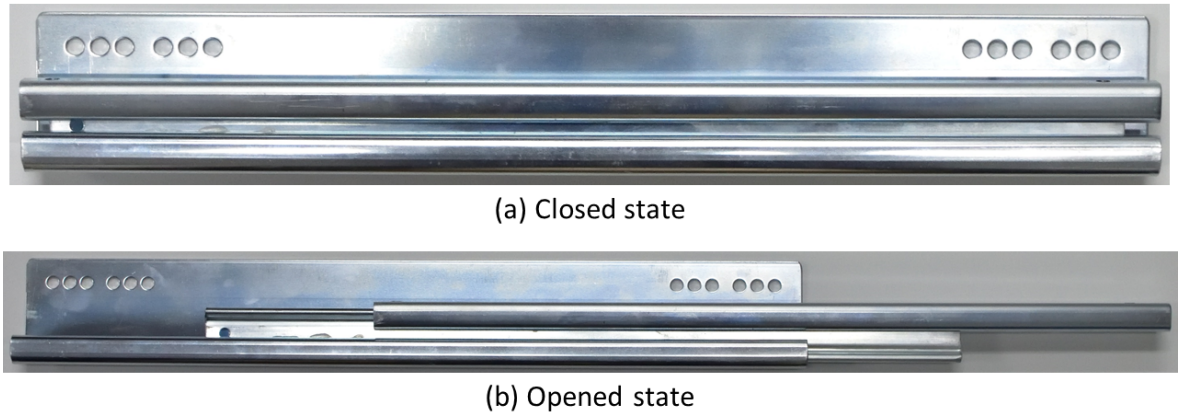

Figure 1. Real slide rail in (a) closed and (b) opened state

During its operational lifetime, the slide rail experience different load conditions which may affect its wear, causing an increase of the end-point deflection of the rail as well of the drawer where the rail is installed. Since excessive deflection of the end-point may result in collision or malfunctions, slide rail producers need to set up rules to define, in a reasonable and quantities way, the operational lifetime of the slide rails based on average loading conditions. For this reason, the wear phenomenon should be firstly measured, by means of material characterization experiments, and afterwards modeled in a numerical simulation, for the quick and precise estimation of the of the end-point deflection and lifetime of the slide rail.

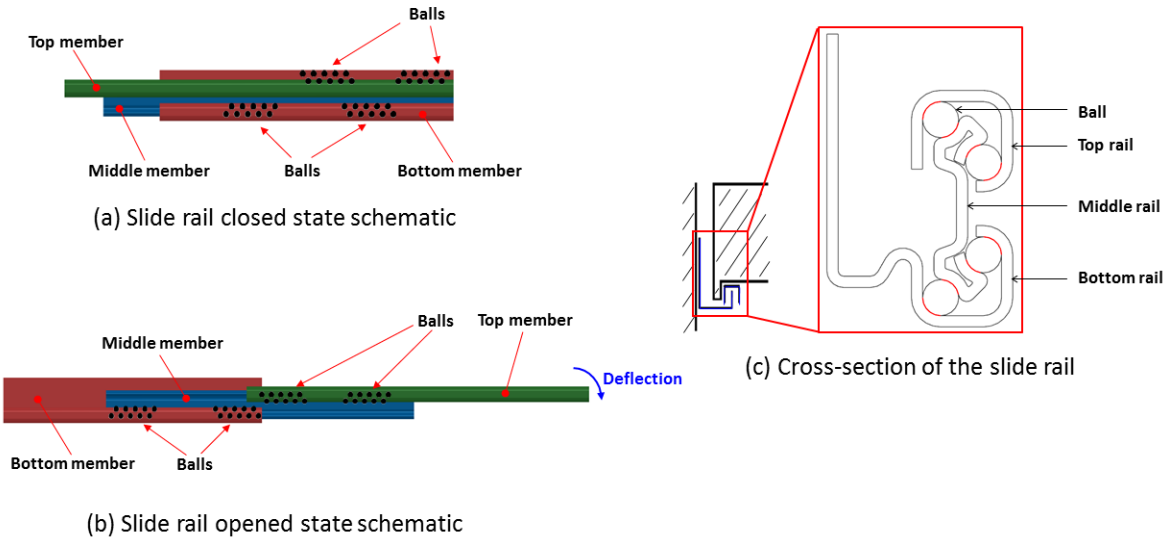

Figure 2. (a) Slide rail in closed (b) and opened state and (c) cross-section detail

3. Theoretical background

As previously anticipated, in the present research work the wear phenomena is subdivided into two different contributions, the linear one and the non-linear one. As shown in Figure 3(a), the application of the Archard model results in a continuous inward movement of the rail surface toward its thickness as a result of the progressive wear. Instead, the consequence of the utilization of the Lemaitre model accounts for the surface element deletion in case the critical damage value is reached, Figure 3(b). The meaning of "element deletion" accounts for the pitting phenomena of the rail surface which is taken into account in the numerical simulation by deleting the elements those reach the critical damage value. Since both these models are utilized in FEM simulation, for the accurate calculation of the surface update due to the wear phenomena, the theoretical backgrounds relevant for both Archard and Lemaitre model are summarized in the following two paragraphs.

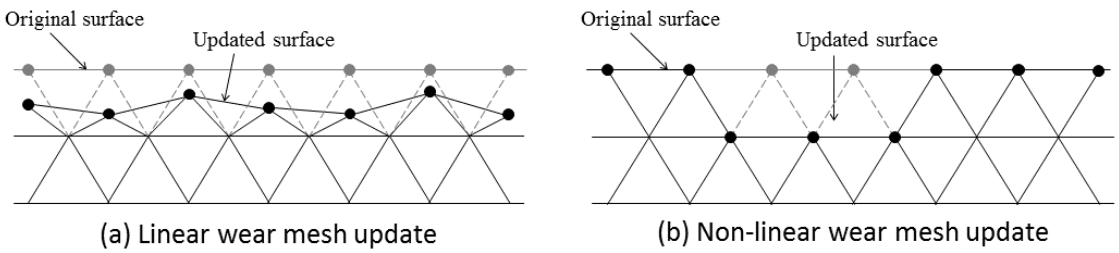

Figure 3. Schematic representation of (a) linear and (b) non-linear wear phenomena

Concerning the linear wear, a modified Archard model is utilized in order to estimate the linear wear along the thickness direction of the rail rather than the total volume loss, as in the original model.

3.1. Archard wear model

The original wear model due to Archard [10] takes into account the amount of volume loss due sliding contact between two material, Eq.(1).

$$Q = \frac{K \cdot W \cdot L}{H} \tag{1}$$

In Eq.(1), Q stands for the total amount of volume loss in the contact surface between the sliding objects; K is a model constants which is determined from the material characterization; W is the normal load applied to the sliding member, which influences the amount of wear, the higher the load the higher the effect of wear. L is the total length of the sliding movement and it is the independent variable in the calculation; as L increases the amount of wear, and accordingly the amount of volume loss, increases as well. Finally, H is the hardness of the considered material, expressed in MPa. In the considered case however, since the linear material loss in the thickness direction of the rail, δ, is meant to be calculated, the modified formulation shown in Eq. (2) is utilized.

$$\delta = \frac{K \cdot W \cdot L}{H \pi r_b l} \tag{2}$$

In Eq. (2), the remaining parameters r_b and l stand for the slide rail ball radius and ball sliding contact distance, respectively. The schematization of the contact is shown in Figure 2(c), where the red lines represent the contact length between balls and rails. According to the original Archard model, on the basis of the progressive increment of the total sliding length L, the amount of the material erosion in the thickness direction of the slide rail increases, following an L-dependent linear path. Since, in some of the analyzed cases, the linear formulation of Eq.(1) and Eq.(2) have shown not to properly fit the experimental data, a modification of the Archard model is proposed and shown in Eq.(3), where the exponent a has been added in order to better model the slight non–linearity in the curves.

$$\delta = \frac{K \cdot W \cdot L^a}{H \pi r_b l} \tag{3}$$

The impact of this modification will be shown in the result section where, especially under heavy load condition, the original Archard model fails to catch to the trend of the experimental data. The material properties K and a are derived from the material characterization experiments made by utilizing the developed test machine, and the relevant test conditions and results are presented in the following paragraph.

3.2. Lemaitre damage model

In the original work due to Lemaitre [11], a thermodynamic model for the estimation of the damage evolution for isotropic materials is proposed. Based on a simple tension test, the critical damage value, over which the material is considered to fail, can be calculated according to Eq. (4), where UTS stands for the ultimate tensile strength of the material under uniaxial loading condition and $\sigma_{break,true}$ for the uniaxial true break stress.

$$D_c = 1 - \frac{UTS}{\sigma_{break,true}} \tag{4}$$

As the damage increases, both the equivalent stress tensor and the deviatoric stress tensor vary according to evolution of the damage, as shown in following Eq. (5) and Eq. (6), respectively. The

value of σ_d and s_d stand for the vectors relevant for the damaged material, whereas σ_{orig} and s_{orig} are those of the undamaged one.

$$\sigma_{orig} = \frac{\sigma_d}{1-D} \tag{5}$$

$$s_{orig} = \frac{s_d}{1-D} \tag{6}$$

In the Lemaitre model, the increment of damage value D, Eq. (7), is influenced by the equivalent plastic strain rate ε_p and by the damage strain released rate *Y*, the last defined as in Eq. (8).

$$D = \varepsilon_p \frac{1}{1-D}\left(\frac{-Y}{S_0}\right)^b \tag{7}$$

$$-Y = \frac{\sigma_{eq,vM}}{2E(1-D)}\left[\frac{2}{3}(1-\nu)+3(1-2\nu)\left(\frac{s_{dev}}{\sigma_{eq,vM}}\right)\right] \tag{8}$$

In Eq. (8) $\sigma_{eq,vM}$, s_{dev}, E and ν stand for von Mises equivalent stress, the deviatoric stress, the Young's modulus and the Poisson ratio, respectively. The ratio between s_{dev} and $\sigma_{eq,vM}$ stands for the triaxiality factor, which represents the amount of off-plane stress in comparison to the von Mises plane stress state. For the determination of the constants to be utilized in the Lemaitre damage model, S_0 and *b* respectively, simple tension test experiments on the material utilized for the realization of the rails have been conducted and are presented in the following paragraph.

3.3. Combined utilization of linear and non-linear wear models

In the present research work, since two different models are used to describe the progressive wear of the material, further explanation of how these approaches are combined together are given in this section of the paper.

Analyzing the increment of the end-point displacement for a slide rail, three different behaviors can be identified, as shown in Figure 4. In case the load applied does not make the material of the rail to reach UTS during the operational lifetime, the value of the end point displacement manifests small variation from the initial static deflection as the number of cycles increase, Figure 4 "curve 1". As it will be shown in the result section, the small variation of the end-point displacement (for high number of cycles) are well modeled by utilizing only the Archard modified model shown in previous Eq. (3).

If the average load increases, as shown by the result "curve 2" in Figure 4, the slide rail manifests two consequent different behaviors. From the static loading to most of its operational lifetime, the wear curve agrees with the Archard modified model but, from a certain point, the slope of the curve abruptly changes and the slide rail experience a critical increase of the end-point deflection in few hundred cycles. The transition between these two behaviors is explained by the fact that a huge portion of the sliding surface of the rail reaches the UTS value and the damage accumulation starts, leading soon after to an inadmissible end-point displacement. For the proper modelization of this phenomenon, an accurate material testing as well as a precise inverse calibration of the material data in the numerical simulation are essential.

Finally, the third and last observed behavior is described by "curve 3" in Figure 4, where the excessive load applied to the slide rail makes the linear wear contribution to be almost negligible and the end-point deflection to abruptly increase from the static load to the failure in few thousand cycles.

Although the number of cycles and loads for which different slide rails models experience these three kind of deflection vs cycles behavior differ, these three patterns seems to be always present and,

as it will be shown in the result section, the combination of the modified Archard model and of the Lemaitre model can successfully describe them.

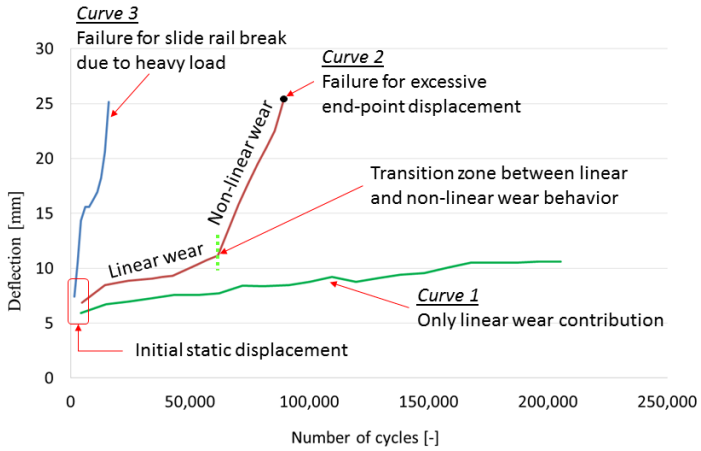

Figure 4. Different wear behaviour patterns

4. Material characterization and model constants determination

In order to properly characterize the basic mechanical properties of the material of the rail guides as well as the wear behaviour due to the interactions between balls and rails, two different tests have been carried out. First, a simple tension test under room temperature conditions for the rail material SCP10 has been conducted utilizing the ASTM E8 standard for the realization of the specimen, as shown in Figure 5. The test has been conducted at 1 mm/min.

The results of the test are shown, in terms of engineering stress-strain, in following Figure 6(a) whereas in Figure 6(b) the true stress-strain curves, together with the fitting obtained by utilizing the Swift model, are reported. The model parameters and material properties obtained from the simple tension test material characterization are reported in Table 1. The Poisson ratio is assumed to be 0.31 according to the SCP 10 (DIN specification 1.0330) material datasheet.

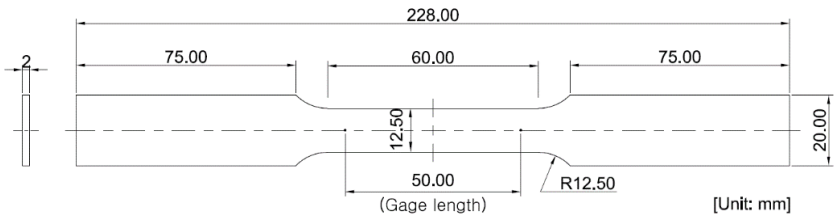

Figure 5. ASTM E8 standard tensile test specimen

In order to properly simulate the material behaviour in the numerical simulation, inverse calibration approach has been utilized to minimize the differences between experimental and numerical stress-strain curve, both in the plastic and in the necking region, as shown in Figure 6a. The constant for the Lemaitre damage model, derived from the inverse calibration of the results of the simple tension test, are summarized in Table 2.

Concerning the determination of the constants of the modified Archard model, the test machine shown in Figure 7 has been designed and built. The machine replicates the operating conditions of the slide rail and, thanks to the encoder placed on the members, speed and displacement can be recorded during the test.

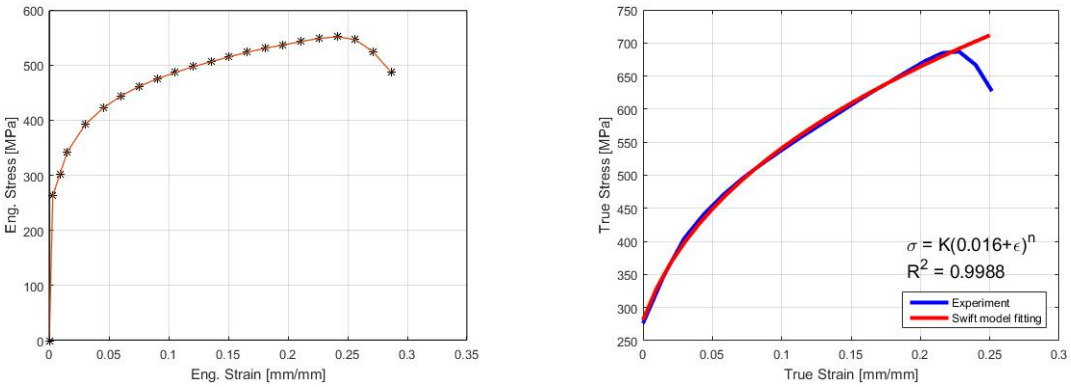

(a) Simple tension test curve (b) Swift model fitting

Figure 6. Simple tension test result (a) and Swift model fitting (b)

Table 1. Results and fitting parameter of the simple tension test for the SCP10 material

Parameter	**Value**	**Description**
E	200 GPa	Young's modulus
σ_{ys}	301.8 MPa	Yield strength
K	690.0 MPa	Swift model constant
ε_0	0.0016	Initial strain
n	0.169	Hardening exponent

Moreover, in order to reduce the overall complexity of the sliding wear test, modified rails with only 4 balls has been realized by the slide rail producer and have been utilized in this test. In principle, the presence of only 4 balls, instead of the original 40, allows reducing to 1/10 the weight to apply on the last member of the rail thus make the experiment to be more manageable and reduces possible undesired inertia-induced failures in the components of the test machine. Afterwards, by correlating the load condition to the number of balls, it is possible to link the results of the test machine with those of the real rails. Balls radius, r_b, and sliding distance, l, there-and-back, are 6.4mm and 200mm respectively.

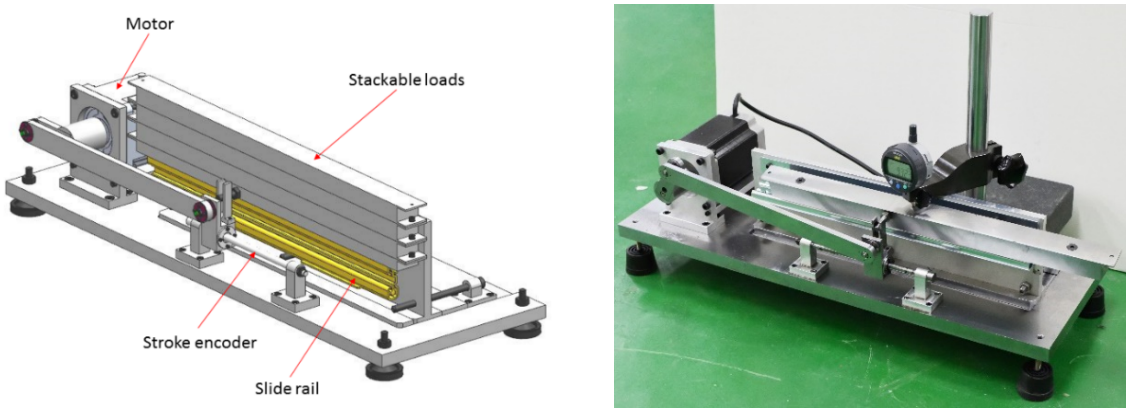

(a) Test machine design (b) Test machine in operation

Figure 7. Slide rail laboratory test machine (a) design and (b) in operation

In order to simulate all the feasible average weight conditions, experiments have been carried out considering different distributed loads on the last member of the slide rail in the test machine, in detail: 4.5kgf, 6.75kgf, 7.875kgf and 9kgf, which correspond to 45kgf, 67.5kgf, 78.75kgf and 90kgf in the real application. In the products where the slide rails are utilized, for instance a drawer, two rails are installed, whereas in the developed test machine one rail is tested and only 4 balls are installed between the members. For instance, in the real application, a weight of 45kg is distributed on two rails, each one having 40 balls, which corresponds to a 0.56kgf load for each ball. In the test machine, since only 4 balls are installed, to replicate the exact test condition, a load of 2.25kgf should be applied but, in order to conduct accelerated tests, a two times higher load has been applied, leading to a distributed load of 4.5kgf, as previously anticipated.

Table 2. Parameters for the wear models

Parameter	**Value**	**Description**
K	$1.039 \cdot 10^{-5} e^{0.1774 \cdot W}$	Archard model constant
a	$-0.0109\,\mathrm{W} + 1.0578$	Archard model constant
S_0	36.4	Lemaitre model constant
b	0.89	Lemaitre model constant
H	81 HB	Rail material hardness

Since the high variation of loads among the experiments, the modified Archard model constants varies from case to case and, for this reason, in Table 2, the fitting equations from which to calculate them are reported. As it will be shown in the results section, for both fitting equation, the coefficient of determination (R^2) have been calculated in a range between 0.95 and 0.99, proving the reliability of the proposed approach, in comparison to the linear model. The fitting equation have been included in the numerical model for a precise estimation of the Archard model constants based on the weight applied to the slide rail. Finally, the remaining constants, to be utilized in both linear and non-linear wear models, are summarized in Table 2.

5. Numerical model implementation

The numerical model, replicating all the assembly product made of three rails and 40 balls, have been realized by utilizing ABAQUS/Explicit. In order to simulate the screws connecting the slide rail to the product where it is utilized, an encastre boundary condition have been applied to all the nodes on the side wall of the rail. For all the various load condition, a distributed load has been applied on the top surface of the last member of the slide rail, as shown in Figure 8.

The model has been meshed utilizing the C3D8R hexaedral, an 8-node linear brick, reduced integration, hourglass control element. The C3D8R allows a fast calculation while assuring precise results, as shown in the previous work of Zou et al. [12] for the roll forming process, Tajyar et al. [13] for the non-circular tube forming process, Cai et al. [14] for the roll forming process, Yang et al. [15] and Guo et al. [16] for the ring rolling process.

The mesh size varies according to different zones; the values of the mesh size in the contact are between balls and rails is set as 0.1mm whereas in the remaining zone, not relevant for the calculation, is set to 20mm.

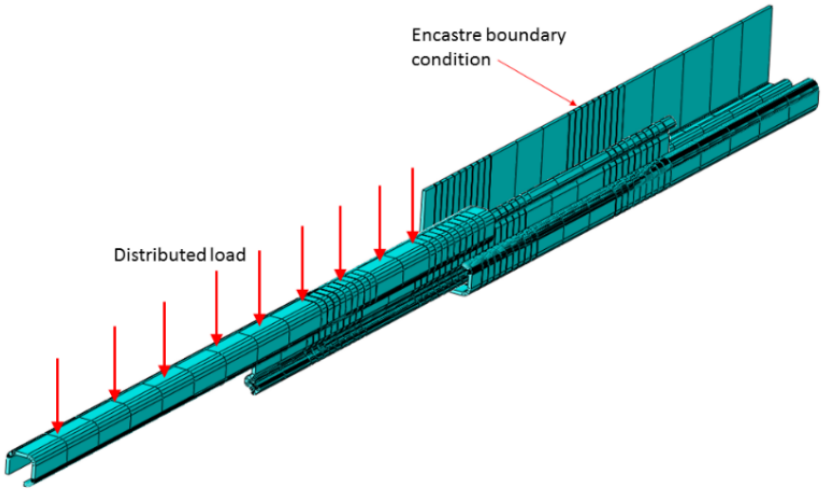

Figure 8. Slide rail numerical model (ABAQUS)

6. Results and discussion

In order to prove the reliability of the modified Archard wear model, the fitting curve relevant for the original one and for the modified one are here after reported, for each one of the four study cases, along with the relevant coefficients of determination. The wear depth amount vs number of cycles curves, along with the interpolation made with the models shown in previous Eq.(2) and Eq.(3), are shown in Figure 9, for the 4.5kg case, Figure 10, for the 6.75kg case, Figure 11 for the 7.875kg and Figure 12, for the 9kg case whereas the relevant coefficients of determination are reported in Table 3.

As it is possible to conclude from the comparison chart and from the coefficients of determination, the modified Archard model is able to better catch the trend of the experimental data and the improvement is as greater as the load applied to the slide rail increases. The reason for this is given by the fact that the higher the load the higher the non-linearity of the displacement vs cycles, resulting in an increasing error if a linear function, as the original Archard model, is used to interpolate the data.

Table 3. Coefficient of correlation comparison between original and modified Archard model

Case	R^2 modified Archard	R^2 original Archard
4.5kg	0.9901	0.8581
6.75kg	0.9516	0.3253
7.875kg	0.9632	0.1589
9kg	0.9939	0.0860

In the numerical simulation, as a consequence of the application of two different wear models, two different update of the surface of the slide rail are present. As previously anticipated, the modified Archard model progressively erodes the surface of the rail whereas the Lemaitre damage model accounts for the surface element deletion, when an element reaches the critical damage.

The critical damage stands for the value over which the material completely fails and cannot withstand any more load, resulting in the detachment of the considered portion of material from the rail. The damage accumulation starts from the UTS point, where the damage accumulation starts, and end in the break point where, according to the Lemaitre damage model, the accumulated damage reaches the unity value.

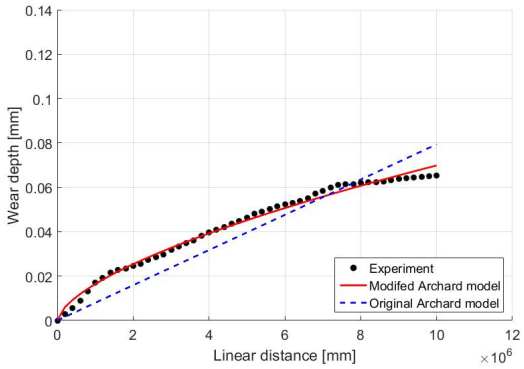

Figure 9. Wear model comparison for the 4.5kg case

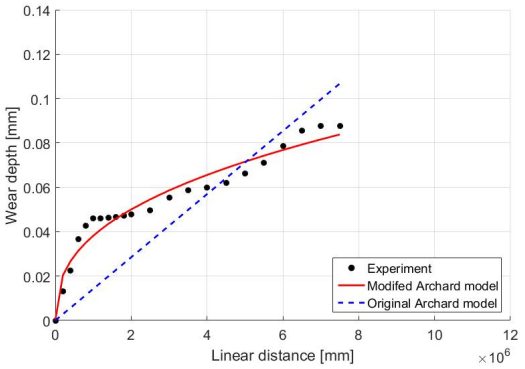

Figure 10. Wear model comparison for the 6.75kg case

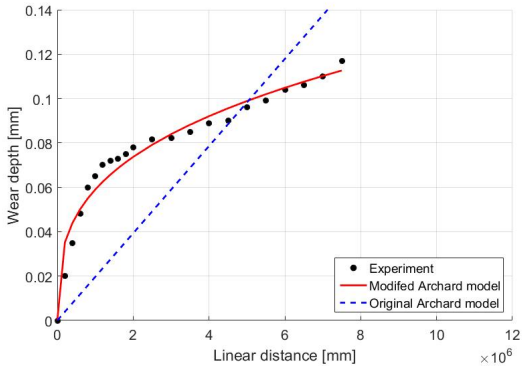

Figure 11. Wear model comparison for the 7.875kg case

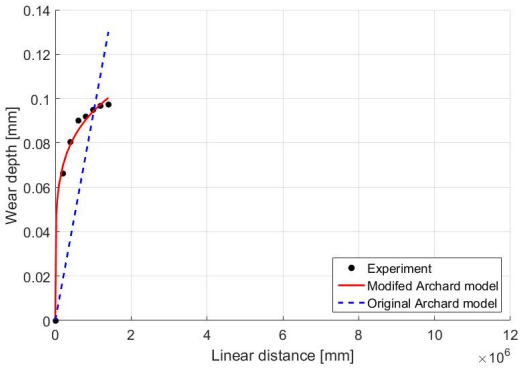

Figure 12. Wear model comparison for the 9kg case

In the numerical simulation, the linear wear contribution is described by an inward movement of the surface nodes, as the number of cycles increases, resulting in a variation of the dimension of the inner part of the rail, while the original shape of the geometry is almost kept constant. On the other hand, when an element reaches the critical damage value in the Lemaitre model, it is deleted from the mesh, resulting in a change of the geometry of the considered portion of the rail, which starts to look scarred. Both this different mesh updates are shown, along with the original surface of the inner part of the rail, in following Figure 13. As a consequence of the progressive surface update due to continuous wear, the gap between balls and rail increases and the end-point deflection of the last member increases as well. In order to show the increment of end-point deflection of the slide rail as the number of cycles increases, in the result shown in Figure 14 where the displacement scale has been doubled in order to allow a better understanding of the deflection.

Finally, in order to prove the reliability of the proposed numerical simulation, the developed model has been utilized for the estimation of the end point deflection for three different loads, 30kg, 45kg and 50kg respectively. The results of the numerical model have been compared with those provided by the slide rail producer and the comparison of the results is shown in Figure 15.

The utilization of a combined wear models approach allows a precise estimation of the sliding wear effect on the rail inner surface, and the error is limited to 9.82% in comparison to the relevant FEM simulation result. It must be noticed that the modified Archard model is able to precisely follow the trend of the experimental results whereas the Lemaitre model presents some inaccuracies, especially in the proximity of the failure.

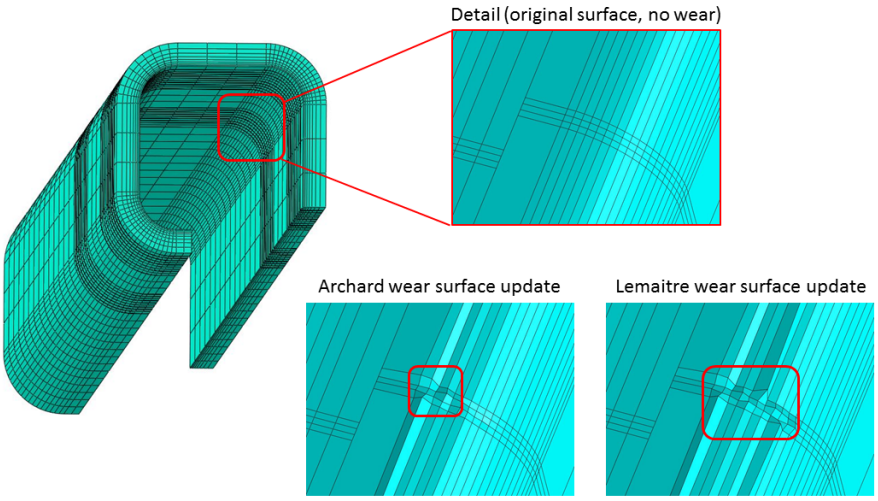

Figure 13. Rail surface update due to Archard and Lemaitre wear models

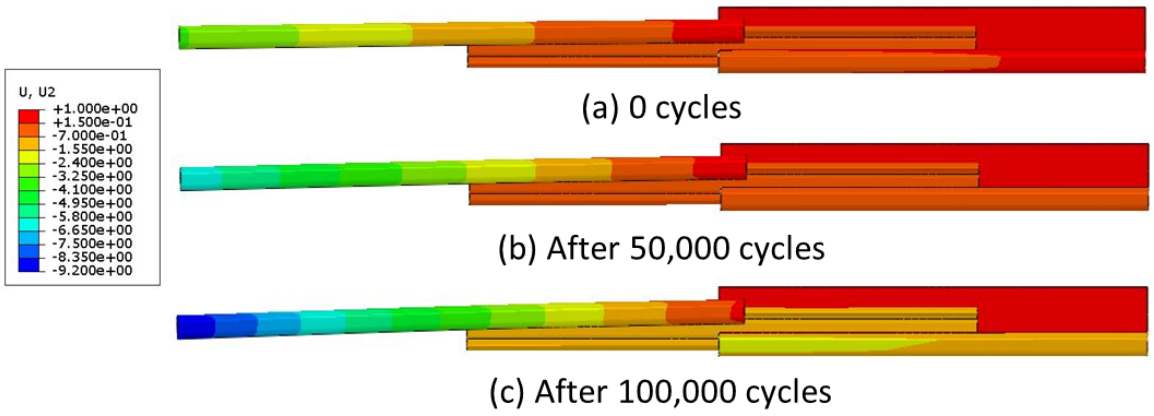

Figure 14. End-point deflection of the slide rail for (a) 0, (b) 50,000 and (c) 100,000 cycles

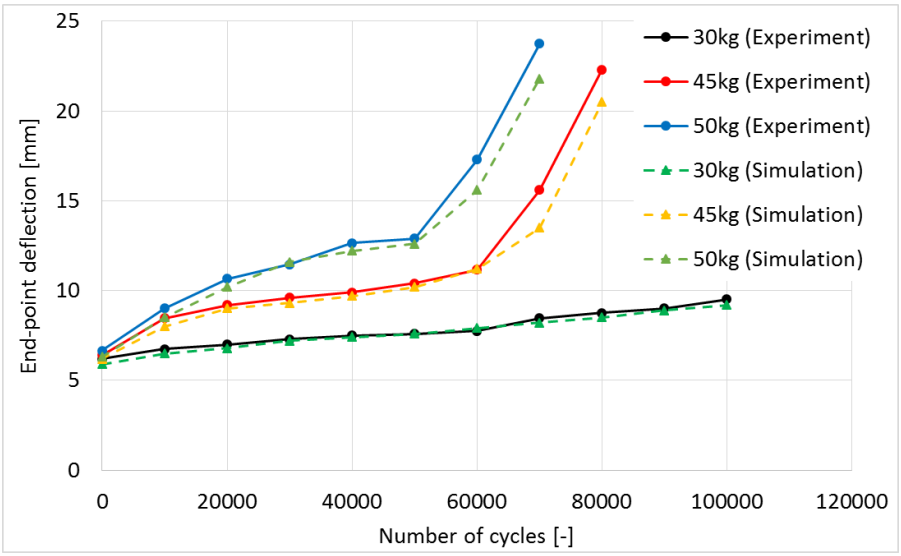

Figure 15. Comparison between simulation and experimental results of the end point deflection

7. Conclusion

In this paper a numerical model for the prediction of the end-point deflection in a slide rail utilized in several white-goods application in proposed. In order to proper account for the wear which occurs in the members of the slide rail due to the sliding contact with the balls, linear and non-linear wear formulations have been utilized and, concerning the linear one, a modified Archard model is proposed and validated, showing how it can well follow the trend of the linear wear occurring during the operational life time.

Finally, the developed model has been applied to three different study case provided by the slide rail manufacturer and its reliability in calculating the end-point deflection, as the number of cycles increase, has been proved.

The developed model is of very interest for the industry since it allows a precise estimation of the increase of wear during the operational life time of rails, and can be extended also to different typology of rails if a proper material characterization is operated.

References

[1] Singh H, Mutyala K C, Evans R D and Doll G L 2015 *Surf. & Coat. Tech.* **284** 281–289
[2] Seo J W, Jun H K, Kwon S J and Lee D H 2016 *I. J. Fat.* **83** 184–194
[3] Feng Y, Huang X, Chen J, Wang H and Hong R 2014 *Mech. Mach. Th.* **81** 94–106
[4] Maru M M, Castillo R S and Padovese L R 2007 *Trib. Int.* **40** 433-440
[5] Nguyen P, Kang M, Kim J M, Ahn B H, Ha J M and Choi B K 2015 *Exp. Sys. App.* 42 9024–32
[6] Karacay T and Akturk N 2009 Trib. Int. 42 836-843
[7] Singh S, Köpke U G, Howard C Q and Petersen D 2014 *J. Sou. Vib.* **333** 5356–5377
[8] Lee N R, Hwang S Y and Kim N S, 2015 *TechConnect W.* 6 21–24
[9] Hwang S Y, Jeong H and Kim N S 2015 *I. J. Mech. & Mechat. Eng.* **15:3** 106-111
[10] Archard J F 1953 *J. Appl. Phys.* **24** 981–988
[11] Lemaitre J 1985 *J. Eng. Mat. Tech.* **107** 83–89
[12] Zou T, Zhou N, Peng Y, Tang D and Li D 2016 *J. Phys. Conf. S.* **734** 032016
[13] Tajyar A and Abrinia K 2009 *I. J. Rec. Tr. Eng.* **1:5** 82–85
[14] Cai Z, Wang M and Li M 2014 *J. Mat. Proc. Tech.* **214** 1820–1827.
[15] Yang H, Guo L, Zhan M and Sun Z 2006 *J. Mat. Proc. Tech.* **177** 634–638
[16] Guo L and Yang H 2006 *Trans. Nonfer Met. Soc.* **16** s645-s651